

# Quantitative experimental studies of spontaneous rotations of bismuth nanoparticles

Avraham Be'er,<sup>1</sup> Richard Kofman,<sup>2</sup> Fritz Phillipp,<sup>3</sup> and Yossi Lereah<sup>1</sup>

<sup>1</sup>*Department of Physical Electronics, Faculty of Engineering, Tel-Aviv University, Tel-Aviv, Israel*

<sup>2</sup>*Laboratoire de Physique de la Matière Condensée, Unité Associée au CNRS No 6622, Université de Nice, Parc Valrose, 06108 Nice Cedex 2, France*

<sup>3</sup>*Max-Planck-Institut für Metallforschung, Heisenbergstr. 3, D-70569 Stuttgart, Germany*

(Received 25 June 2006; revised manuscript received 3 October 2006; published 28 December 2006)

A phenomenon of spontaneous rotations of Bi nanoparticles is reported. Fourier transform (FT) analysis of the high resolution electron microscopy (HREM) images indicates that the rotations occur by plane after plane gliding rather than a collective movement of the entire particle as a rigid body. The phenomenon rate was studied quantitatively by time resolved transmission electron microscopy (TEM). The origin of the phenomenon as a radiation effect of the high voltage electron beam was excluded by finding the same rates at 200 kV and 1250 kV electron beams, below and above the threshold for the knock-on process. The dependence of phenomenon rate on the particles' size was found to be inversely proportional to the particle volume, with a threshold at particle radius of 5 nm. The temperature was found to activate both the probability for a particle to be in the rotating state, and the rotation rate.

DOI: [10.1103/PhysRevB.74.224111](https://doi.org/10.1103/PhysRevB.74.224111)

PACS number(s): 61.50.-f

## I. INTRODUCTION

The recent activity in nanoscale science and technology calls for understanding and controlling the movement of nano-objects [e.g. (Refs. 1 and 2)], particularly their response to random external forces. Applying an external force on a macro-object will result in a combination of a rigid body movement (translation or rotation) and a strain (elastic or plastic). However, for atomic scale objects, terminology of Brownian motion, chemical reaction, and chemical bonding is more appropriate to describe their relation with external fields and forces. Nano-objects, which are of intermediate scale, were found to exhibit unusual properties while exposed to external fields and forces. While carbon nanotubes have extraordinary mechanical properties,<sup>3</sup> the results reported here suggest that metallic nanoparticles should be considered as soft matter. The response of metallic nanoparticles to temperature is known to be different from bulk, e.g., lowering of the melting point,<sup>4</sup> enhanced surface melting,<sup>5,6</sup> and spontaneous rearrangement of the atomic configurations.<sup>7,8</sup> The phenomenon of rearrangement of gold nanoparticles, under the transmission electron microscope (TEM) beam, was first described qualitatively by Iijima and Ichihashi.<sup>9</sup> Howie<sup>10</sup> and Williams<sup>11</sup> suggested that the phenomena is correlated with the high energy electron beam, while Ajayan and Marks<sup>12</sup> correlated the phenomena with temperature by quantitative theoretical studies. In this paper we shed light on the dynamics of the phenomenon by quantitative experimental studies of Bi nanoparticles.

## II. EXPERIMENTAL SETUP

Bismuth particles embedded in amorphous SiO were prepared by successive thermal evaporation in UHV of 5 nm SiO (silicon monoxide SiO<sub>x</sub>, with  $x \sim 1$ ), 8 nm (as an average thickness) Bi, and 10 nm SiO. The element's crystallographic structure is the rhombohedral symmetry  $R\bar{3}m$  (No. 166),<sup>13</sup> with  $a_1 = a_2 = a_3 = 4.745$  Å and  $\alpha = 57.24^\circ$ , and two at-

oms in a unit cell, one at the origin (0,0,0) and one on the major diagonal [see also Fig. 1(d)]. This is essentially different from previous FCC elements, such as Au and Pb, studied in the past.<sup>7-12,14</sup> Bi particles in various diameters in the range of 2–50 nm were formed between the two SiO layers. Large Bi particles ( $\sim 20$  nm and above) are inclined to be elongated rather than circular. The bigger the particle is, the larger the deviation from the sphere. Embedding the particles in SiO ensures better thermal coupling, which defines good thermodynamical variables and prevents oxidation, migration, and evaporation.<sup>15</sup>

The specimens were examined by transmission electron microscopy at 200 kV (Philips F20) at various temperatures, down to liquid nitrogen temperature (LNT), using a cold stage (Gatan 900), by high resolution transmission electron microscopy (HREM), and by dark field (DF) microscopy. HREM observations at room temperature were obtained also at 1250 kV (JEM-ARM1250). The structure evolution of the particles was video recorded by an electron sensitive video camera (Gatan 622 SC) with a time resolution of 25 frames per second. The records were examined frame by frame using Premiere software; fast Fourier transform (FFT) of the single frames was obtained by MATLAB and by Scion Image software.

## III. RESULTS

### A. High resolution electron microscopy (HREM)

The HREM measurements were mainly focused on Bi particles with a diameter of about 10 nm, at room temperature. Two states exist for a particle: (a) Stable state, and (b) Rotating state. Each particle stays in each state a characteristic time scale of tens of seconds and then switches to the second state. The particles fluctuate between the two states several times during the experiment, which lasts a few minutes. At room temperature, the Bi particles stay mostly (80%) in the rotating state. During the rotating state, the particles

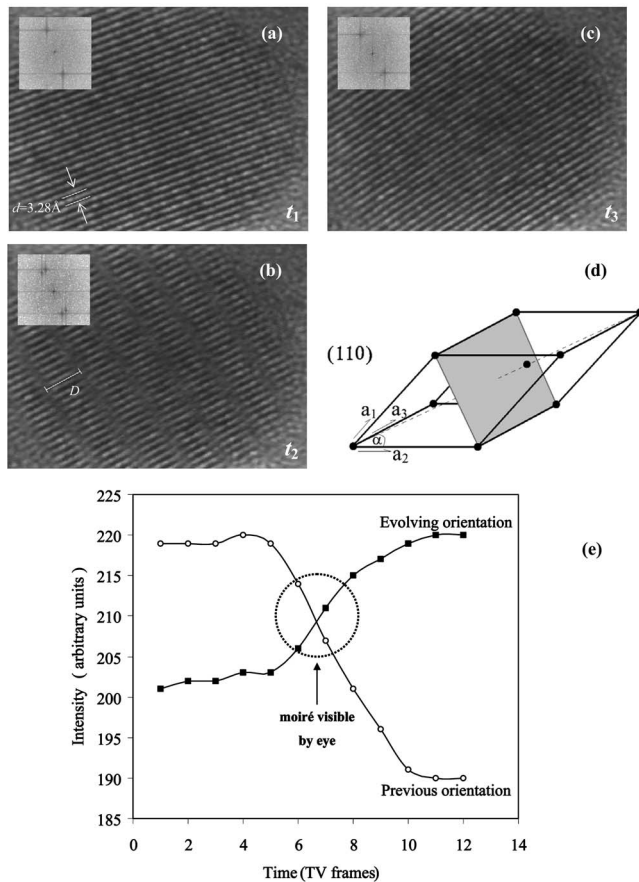


FIG. 1. The rotation phenomenon. (a–c). A sequence of three snapshots with relevant FFT showing a rotation of the (110) planes by  $\theta=11.5^\circ$ . The time interval between successive snapshots is 0.12 s (3 TV frames). The intermediate snapshot,  $t_2$ , shows moiré fringes and its FFT pattern combining the two orientations, the previous one (related to  $t_1$ ), and the evolving one (related to  $t_3$ ). (d) The figure describes the rhombohedral Bi cell and the relevant (110) plane. (e) The intensity of the FFT spots related to (110) planes of the two orientations during the rotation (in this case by  $14^\circ$ ). The intensity of the evolving direction increases monotonically while the intensity of the previous direction decreases monotonically. The moiré pattern is visible when the intensity of both directions is similar.

change their crystallographic orientation spontaneously and continuously at a rate of 2–5 events per second. Particles larger than 10 nm (in diameter) do not show spontaneous rotations, whereas much smaller particles are fluctuating, at room temperature, faster than the video camera is able to resolve by the HREM method.

The process of rotation is demonstrated in Fig. 1 as follows: Figs. 1(a) and 1(c) are initial and final states, respectively, showing that in this particular example the (110) planes are rotated by an angle of  $\theta=11.5^\circ$ . Figure 1(b) is an intermediate stage, showing a moiré pattern which combines both orientations of (110) planes as is indicated by the FFT insert. The moiré patterns during the rotations were found to satisfy the rotational moiré relation:  $D=d/2 \sin(\theta/2)$  where  $D$  is the moiré spacing,  $d$  is the (110) lines space, and  $\theta$  is the angle of rotation. The images of the moiré patterns were

studied using the Fourier analysis: Figure 1(e) shows the evolution of the intensity of the FFT spots of a rotating particle, in this particular case by  $14^\circ$  during 7–8 TV frames. In all cases, the intensities of the FFT spots are changed continually with a characteristic time of 0.04–0.5 s corresponding to 1–12 frames. While the intensity of the spots related to the previous orientation decreases, the intensity of the spots related to the new orientation increases. The moiré pattern is visible by eye [see Fig. 1(b)] when the intensity of both directions is similar. Results of a field-by-field analysis (a TV frame is created by two intercalated fields) are compatible with this analysis, indicating that no intercalation phenomena are involved. The monotonic behavior seen in Fig. 1(e) indicates that the particle rotates by gliding layer-by-layer, as more layers rotate the intensity of the evolving direction becomes dominant over the previous one. The monotonic behavior excludes an interpretation that the moiré pattern is a result of fast (faster than one TV field interval) switching between the two states. Observations of the phenomenon at an exact zone axis indicate that the direction of motion of the rotated layer is normal to  $(\bar{1}11)$  plane. The particle rotation is illustrated in Fig. 2.

Several particles (5–10) of diameter 10 nm were examined in detail by HREM; from these particles, about 100 visible transitions, on the plane normal to the  $e$  beam, were analyzed, in order to find the distribution of the angular rotation  $\theta$  between the (110) atomic planes of succeeding configurations. Rotations by all angles up to  $40^\circ$  were observed, most of them at angles below  $15^\circ$ , with a typical average value of  $8^\circ$ , with no preference of a specific angle. It should be noted that rotations occur not only on the plane normal to the electron beam. However, the angles of such rotations cannot be quantified because the particle does not remain in Bragg condition during the rotation process.

## B. Dark field (DF) microscopy

The dynamics of particles of different sizes (4.7–10 nm in diameter) was analyzed at different temperatures using dark field (DF) microscopy. The DF microscopy is obtained at a low magnification; therefore statistical analysis is reliable as many particles are included in the field of view. The DF aperture was positioned on the ring corresponding to (110) reflections. In the DF method, rotations of the particles around the beam axis are visible when the diffracted beam crosses the DF aperture's borders, or alternatively, if the particles rotate around an axis perpendicular to the beam axis and go in and out of the Bragg condition. The rotation rate observed by the DF is about 10 times smaller than the rotation rate observed by HREM, indicating that most events of rotations are around the beam axis, as explained in Ref. 16, in compatibility with the HREM observations. The rotation rate is found to depend on the particle size; the smaller the particle is, the higher the rotation rate is. The dependence of rotation frequency  $f$  vs particles size was plotted as a function of various powers of the particle radius  $R$ , revealing the best fitting factor (based on the square of the sample correlation function of the linear fit) for the power of 3 [insert of Fig. 3(a)]. Figure 3(a) shows the rotation frequency obtained

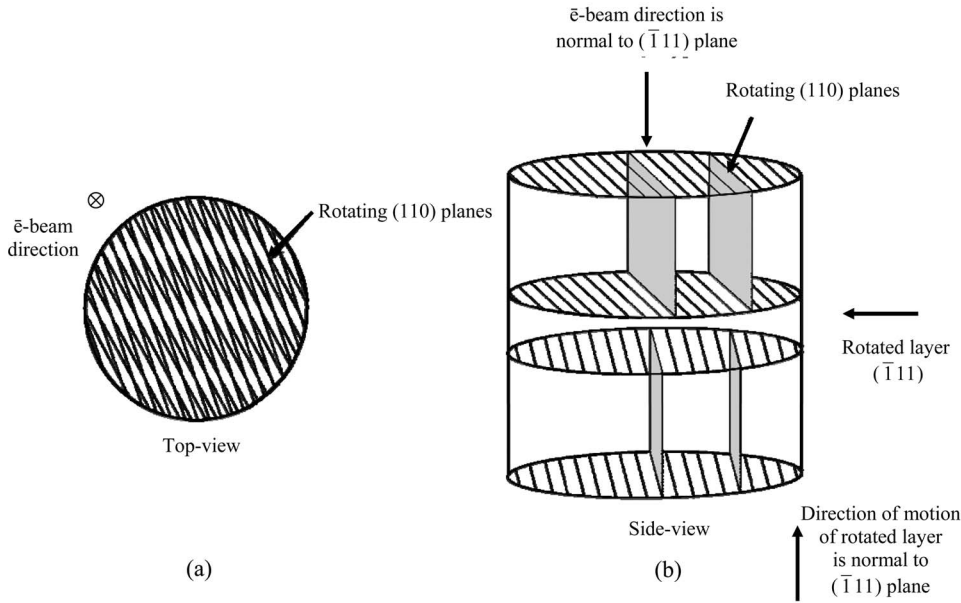


FIG. 2. The crystallographic sketch of the rotation process: (a) A schematic top-view of the particle reveals the moiré pattern as the (110) planes of both parts of the particle interfere. (b) A schematic side view of a rotating particle. The set of parallel lines and the dark planes are the (110) rotating planes. During the visible rotations, the rotated layer moves normal to the electron beam direction.

by the DF microscopy as a function of  $1/R^3$  for various temperatures. A cutoff of the rotation rate at the particle diameter of 10 nm independently on temperature is observed. The following relation reflects the characteristic length scale of the phenomenon:

$$f(R) = C(T) \begin{cases} 1/R^3 - 1/R_0^3 & R < R_0 \\ 0 & R \geq R_0, \end{cases} \quad (1)$$

where  $R_0 = 5$  nm.  $C(T)$  is a temperature dependent constant which together with  $f_0$ , presented in Fig. 3(a), are discussed below.

While quantifying the dependence of the phenomenon on the temperature, a deviation of the actual temperature, at the region under observation from the measured one, is considered. Two origins exist for the deviation: the electron beam used for observation that heats locally the region under study, and the poor heat conductivity of the thin film. Both effects result in increasing the temperature at the observed region. Based on the discrepancy between the measured melting temperature of Ga and the real one, and the discrepancy between the evaporation temperature of ice under the beam and far from it, the following is estimated as required corrections: additional 10 °C and 60 °C at room and liquid nitrogen temperatures, respectively.

Two distinct parameters were found to depend on temperature: (a) The probability  $p$  of a particle to be in the rotating state; the higher the temperature is, the longer the rotating state, and (b) The rotation frequency  $f$ , while in the rotating state; the higher the temperature is, the higher the rotation rate is.

With regard to the probability of the particles to be in the rotating state, and based on the above estimated corrections, it was found that particles stay in the rotating state at RT and at  $-120$  °C, 80%, and 5% of the time, respectively. Considering that the probability of a particle to be in the rotating state is thermally activated  $p = p_0 \exp(-\Delta E_p/kT)$ , the depen-

dence of  $p$  on the temperature indicates an activation energy  $\Delta E_p$  of  $0.08 \pm 0.02$  eV.

Considering that the rotation rate  $f$ , during the rotating state is also thermally activated

$$f(T) = f_0 \exp(-\Delta E_f/kT), \quad (2)$$

the dependence of the rotation rate on the temperature indicates an activation energy  $\Delta E_f$  of 0.01–0.02 eV independently of the particle radius [see Fig. 3(b)], where  $f_0$  is the maximal frequency for a given particle of radius  $R$ . The value of  $f_0$  was found from Eq. (2), as an average, by substituting various measured values of  $f$  and  $T$ , for each  $R$ . It was found that also  $f_0$  is proportional to  $1/R^3 - 1/R_0^3$  [see Fig. 3(a)]; accordingly we conclude that  $f(R, T) = A_0 f(R) f(T)$  where  $C(T)$  in Eq. (1) is  $\exp(-\Delta E_f/kT)$  thus

$$f(R, T) = A_0 \exp(-\Delta E_f/kT) \begin{cases} 1/R^3 - 1/R_0^3 & R < R_0 \\ 0 & R \geq R_0, \end{cases} \quad (3)$$

where  $A_0$  is a constant.

The phenomenon was observed also with an electron microscope operated at 1250 kV. HREM at room temperature of 10 nm Bi particles shows the same rotation rate of 2–5 Hz, as observed with the electron microscope operated at 200 kV. In addition, at 1250 kV, the Bi particles were found to stay in the rotating states for the same characteristic time scale of tens of seconds, mostly (80%), similarly as for 200 kV. The threshold energy  $E_t$  for the knock-on processes is determined according to the formula<sup>17</sup>

$$E_t = \frac{\left(\frac{100 + AE_d}{5}\right)^{1/2} - 10}{20}, \quad (4)$$

where  $A$  is the atomic weight,  $E_t$  is in MeV, and the displacement energy  $E_d$  is in eV. Following Ref. 18, the displacement energy of Bi is 13 eV and thus the threshold energy is around 680 keV. Our experiments show using the electron beam be-

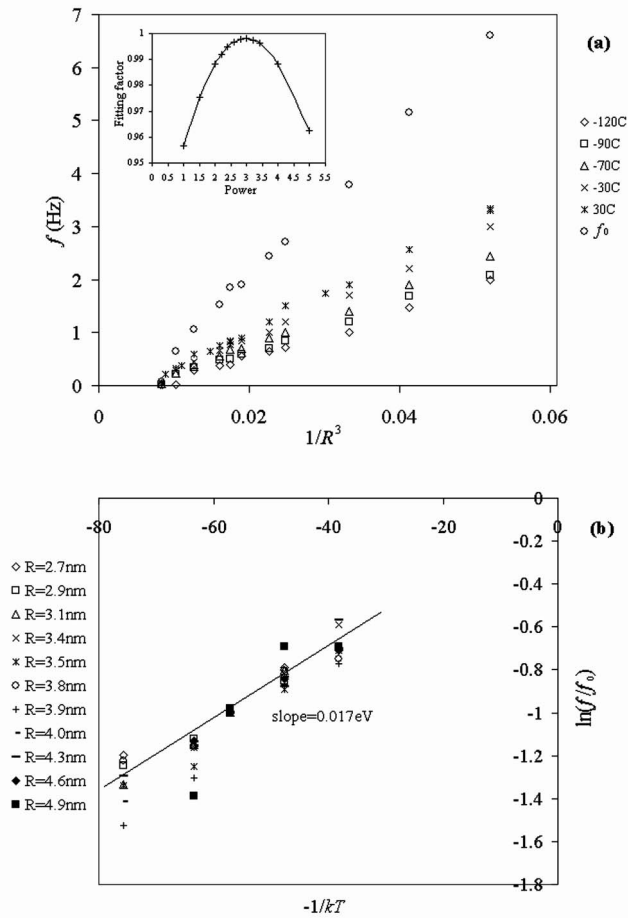


FIG. 3. Quantitative characterization of the rotation frequency. (a) Rotation frequency measured by the DF as a function of  $1/R^3$  for several temperatures: 30 °C, -30 °C, -70 °C, -90 °C, and -120 °C, where  $f_0$  is the maximal frequency for a given particle with a radius  $R$ , calculated from Eq. (2). The cutoff at the particle diameter of 10 nm is independent on the temperature, implying a characteristic length scale in the system. Insert: The accuracy of fitting a straight line to the graph of  $f$  vs  $1/R^\alpha$  for various values of  $\alpha$ . (b) Linear behavior of  $\ln(f/f_0)$  as a function of  $-1/kT$ , for different particles of different radii with the same slope of  $\Delta E_f = 0.017$  eV, implying that  $f = f_0 \exp(-\Delta E_f/kT)$ .

low and above the threshold for the knock-on process does not influence the characteristic time scale of the phenomenon. The origin of the phenomenon as a radiation effect of the high-energy electron beam is thus excluded.

#### IV. DISCUSSION

The phenomenon of spontaneous changes in the structure of small particles was observed mainly in Au,<sup>8,9</sup> and in Pb (Ref. 7) nanoparticles. Spontaneous rotations of small particles appear during epitaxial growth also, and were considered as a recrystallization process,<sup>19</sup> but to our best knowledge no mechanism is proposed. While Ajayan and Marks<sup>12</sup> considered the phenomenon of spontaneous structural changes as a “quasimelted” state, Ben David *et al.*<sup>7</sup> found that the phenomenon is correlated with the movement of

twin defects, which are known to extensively exist in these FCC nanoparticles. Here we show that the phenomenon of structural spontaneous changes exist in Bi nanoparticles also, despite the fact that no twins exist. In the Bi particles the rotations are found to be correlated with plane after plane gliding process similar to plastic deformation of materials under stress. It is proposed that in the case of nanoparticles surface stresses exist. These stresses are roughly estimated based on Laplace pressure relation:  $\sigma = 2\gamma/R$ , where  $\gamma$  is the surface tension and  $R$  is the particle radius. Following this relation, for a 5 nm Bi particle and  $\gamma \sim 400$  erg/cm<sup>2</sup>,<sup>20</sup> the expected stress is of the order of  $10^9$  dyne/cm<sup>2</sup>. Such a stress is typical for bulk elastic-inelastic strains transition<sup>21</sup> and explains the existence of the threshold in particle size for the reported phenomenon. This means that below a characteristic particle radius, and for a given material, plastic deformations can spontaneously cross the particle and cause rotations. Moreover, the velocity in which the rotated layer crosses the particle was found to be of the order of  $10^{-8}$  m/s, which is compatible with shear strain velocities at the same external stresses of  $10^9$  dyne/cm<sup>2</sup>.<sup>22</sup>

Ajayan and Marks<sup>12</sup> have proposed a scheme showing a deep energetic well followed by shallow ones. The particle, in their schematic description, is trapped in the deep well and once out of the well can hop easily over the shallow morphological potential-energy surfaces. Adapting their idea, the energy gap  $\Delta E_p = 0.08$  eV between the stable and rotating states is the deep well, and  $\Delta E_f = 0.01-0.02$  eV is the shallow well, while the particle is in the rotating state. Quantitatively we show that for Bi nanoparticles  $\Delta E_p/\Delta E_f \approx 6$ . The calculated activation energies (0.08 eV and 0.017 eV), compared with 0.025 eV of room temperature, indicate that the driving force stems from the ambient temperature.

It should be noted that the above energies are much below the energy of the planar defects involved in the plane after plane rotation. This energy is estimated to be 50 eV per particle. The estimation is based on considering typical grain boundary energy of the order of 100 erg/cm<sup>2</sup>,<sup>23</sup> and a particle of 10 nm in diameter. This internal energy of 50 eV is a fraction of the surface energy of the entire particle estimated to be in the order of 800 eV. While the particle is stable, this energy is located on the particle’s surface. However, once thermally activated by  $\Delta E_p = 0.08$  eV, the surface energy of 800 eV is redistributed to include a planar defect of 50 eV inside the particle.

#### V. SUMMARY

In summary, we have shown that Bi nanoparticles rotate spontaneously by gliding layer-by-layer and not as rigid bodies. The rearrangements of these nanoparticles can be thus explained by solid-state transitions, and not by melting for a short time period as suggested by Williams.<sup>11</sup> The origin of the phenomenon as a radiation effect of the high-energy electron beam was excluded. The rotation rate was found to be inversely proportional to the particle volume, up to a threshold size, above which the particles are stable, due to lower surface stresses. The temperature was found to activate both the probability for a particle to be in the rotating state, and

the rotation rate. The response of condensed matter to a shear stress is one of the criteria distinguishing solidlike and liquidlike states. Our results suggest that due to the nanometer scale, the response of nanometallic crystals to shear stresses do not show solidlike characteristics such as rigid body rotation. Thus, these metallic nanoparticles may be regarded as “soft matter” and could be used in nanomachines with an equivalent role such as rubber in macromachines.

#### ACKNOWLEDGMENTS

We thank M. Deutsch, W. Kaplan, Y. Kauffmann, and H. Dosh for useful discussion, and R. Höschel for assisting with the high-voltage electron microscopy. This work was supported by the German Israeli Foundation (GIF). A.B. thanks the Israeli Ministry of Science for their support.

- 
- <sup>1</sup>R. Dean Astumian, *Science* **276**, 917 (1997).  
<sup>2</sup>M. Porto, M. Urbakh, and J. Klafter, *Phys. Rev. Lett.* **84**, 6058 (2000).  
<sup>3</sup>A. Krishnan, E. Dujardin, T. W. Ebbesen, P. N. Yianilos, and M. M. J. Treacy, *Phys. Rev. B* **58**, 14013 (1998).  
<sup>4</sup>Ph. Buffat and J-P. Borel, *Phys. Rev. A* **13**, 2287 (1976).  
<sup>5</sup>Y. Lereah, R. Kofman, J. M. Penisson, G. Deutscher, P. Cheyssac, T. Ben David, and A. Bourret, *Philos. Mag. B* **81**, 1801 (2001).  
<sup>6</sup>D. Beaglehole, *J. Cryst. Growth* **112**, 663 (1991).  
<sup>7</sup>T. Ben-David, Y. Lereah, G. Deutscher, J. M. Penisson, A. Bourret, R. Kofman, and P. Cheyssac, *Phys. Rev. Lett.* **78**, 2585 (1997).  
<sup>8</sup>L. D. Marks, *Rep. Prog. Phys.* **57**, 603 (1994).  
<sup>9</sup>S. Iijima and T. Ichihashi, *Phys. Rev. Lett.* **56**, 616 (1986).  
<sup>10</sup>A. Howie, *Nature (London)* **320**, 684 (1986).  
<sup>11</sup>P. Williams, *Appl. Phys. Lett.* **50**(24), 1760 (1987).  
<sup>12</sup>P. M. Ajayan and L. D. Marks, *Phys. Rev. Lett.* **63**, 279 (1989).  
<sup>13</sup>Leonard G. Barry, *Powder Diffraction File* (Joint Committee on Powder Diffraction Standards, Philadelphia, 1974), Inorganic Volume.  
<sup>14</sup>W. Krakow, M. Jose-Yacaman, and J. L. Aragon, *Phys. Rev. B* **49**, 10591 (1994).  
<sup>15</sup>R. Kofman, P. Cheyssac, R. Garrigos, Y. Lereah, and G. Deutscher, *Z. Phys. D: At., Mol. Clusters* **20**, 267 (1991).  
<sup>16</sup>As a typical rotation around the beam axis is 8°, and as the aperture covers about 30° out of possible 360°, only 10% of rotations around the beam axis will be detected by the DF method.  
<sup>17</sup>David B. Williams and C. Barry Carter, *Transmission Electron Microscopy—Basics I* (Plenum Press, New York, 1996), p. 63.  
<sup>18</sup>P. Bois and F. Beuneu, *J. Phys. F: Met. Phys.* **17**, 2365 (1987).  
<sup>19</sup>M. G. Stowell, in *Epitaxial Growth*, edited by J. W. Matthews (Academic Press, New York, 1975), part B, p. 437.  
<sup>20</sup>R. Lide, *Handbook of Chemistry and Physics*, 70th edition (CRC Press, Florida, 1989).  
<sup>21</sup>William F. Smith, *Principles of Material Science and Engineering*, 2nd edition (McGraw-Hill, Singapore, 1990).  
<sup>22</sup>Derek Hull, *Introduction to Dislocations*, 1st edition (Pergamon Press, Glasgow, 1965).  
<sup>23</sup>Van Vlack, *Materials Science for Engineers* (Addison-Wesley, Michigan, 1970).